energy&fuels

Article

Cite This: Energy Fuels 2017, 31, 11253-11257

pubs.acs.org/EF

Catalytic Combustion of Heavy Oil in the Presence of Manganese-Based Submicroparticles in a Quartz Porous Medium

Andrey V. Galukhin,* Mohammed A. Khelkhal, Alexey V. Eskin, and Yuri N. Osin

Kazan Federal University, 18 Kremlevskaya str., Kazan 420008, Russian Federation

ABSTRACT: We synthesized manganese oxide(II) submicroparticles stabilized with oleic acid and used them as oil-dispersible catalyst precursor promoting a heavy oil oxidation process. Size, morphological properties, as well as composition of the catalyst were studied in depth by X-ray phase diffraction analysis, thermogravimetric−mass spectrometry analysis, scanning electron microscopy, energy dispersive X-ray analysis, and nitrogen adsorption measurements. We applied nonisothermal kinetic analysis coupled with an isoconversional approach to study the influence of catalyst on the combustion process and showed that Mn-based submicroparticles accelerate predominantly the high-temperature oxidation process.

1. INTRODUCTION

Smoldering combustion of organic matter dispersed in porous media is a wide-spread phenomenon in nature. For instance, smoldering of the forest ground, peatlands, and coal mines leads to terrible implications and may cause significant environmental problems.[1] Besides the aforementioned negative cases, smoldering combustion in oil reservoirs, well-known as in situ combustion (ISC), is a promising approach to development of oilfields. During ISC, air is injected into a reservoir to oxidize a small portion of the hydrocarbons and generates heat and pressure that enhance oil recovery. Stability of the smoldering front is considered to be a key parameter determining success of the ISC process.[2] One of the possible ways to increase stability of the combustion front is application of catalysts, which can promote the oxidation process and improve oil properties.[3]

Manganese-based catalysts stand out of the row of the catalysts made of other transition metals because of their high catalytic activity for both full[4,5] and partial[6,7] oxidation of organic matter, low toxicity, and availability. This set of properties makes Mn-based catalysts excellent candidates to facilitate smoldering combustion of organic matter.

In our previous study[8] we showed that catalytic species formed from manganese(III) acetylacetonate precursor significantly accelerate combustion of heavy oil. We proposed an approach based on combination of X-ray phase diffraction analysis (XRPD), thermogravimetry, and electron paramagnetic resonance spectroscopy (EPR) to reveal that catalytic cycle includes transitions of manganese between II and III oxidation states. We also showed that initial organic chelate complex transforms into inorganic manganese oxide particles which further participate in the oxidation process.

The current study is a next logical step in our systematic investigation of catalytic oil combustion. We prepared oleophilic manganese(II) oxide submicroparticles and studied their influence on heavy oil combustion. The choice of submicro-sized particles as a form of a catalyst was based on a simplicity of the synthesis and isolation, as well as higher aggregation stability in solutions compared with nanoparticles.

2. EXPERIMENTAL SECTION

2.1. Materials. The crude oil used in this research was extracted from an oil core taken from the Ashalcha oilfield (Volga-Ural basin, Republic of Tatarstan, Russia).[9,10] The physical properties and elemental and SARA (saturated and aromatic hydrocarbons, resins, and asphaltenes) analysis data of crude oil are given in Table 1. All organic solvents were purchased from a local company and used without additional purification (purity was more than 99.5%). Oleic acid (technical grade, 90%) and manganese(II) nitrate tetrahydrate (99%) was purchased from Sigma-Aldrich. Quartz sand was purchased from PJSC "Gusevskiy Glassworks named after Dzerzhinsky".

2.1.1. MnO Submicroparticle Preparation. Initial manganese(II) oleate was synthesized according to a well-known procedure.[11] In a Parr Instrument 4560 autoclave, 13.87 g (22.4 mmol) of synthesized manganese(II) oleate was mixed with 3.50 g (12.4 mmol) of oleic acid and 180 mL of heptane. The resulting mixture was flushed with nitrogen and then heated to 300 °C at a heating rate of 5 °C/min with constant stirring. Then the mixture was held at that temperature for 30 min then slowly cooled to room temperature. The particles were isolated from reaction mixture by centrifugation, washed several times with heptane and methanol, and dried in nitrogen flow.

2.1.2. Sample Preparation for Kinetic Analysis. Samples for TG analysis were prepared by mixing the heavy oil (10.0 wt %) with pure quartz sand ((fraction of 43−64 μm), 90.0 wt %). In the case of catalytic experiments, an initial oil sample contained 2.0 wt % submicroparticles.

2.2. Methods. *2.2.1. Thermal Analysis.* TGA and DSC experiments were carried out with thermal analyzer Netzsch STA 449 F3 Jupiter. The experiments were conducted at linear heating rates of 5, 10, 15, and 20 °C/min for kinetic analysis of heavy oil samples, under air flow (50 mL/min). The samples were heated from ambient temperature to 600 °C. An average sample was 10 mg for each run.

2.2.2. Scanning Electron Microscopy and Energy Dispersive X-ray Analysis. Scanning electron microscopy (SEM) measurements and energy dispersive X-ray analysis (EDX) were carried out by using a field-emission high-resolution scanning electron microscope Merlin Carl Zeiss equipped with an energy dispersive spectrometer AZtec X-MAX. Observation photos of morphology surface were obtained at an accelerating voltage of incident electrons of 15 kV and current probe of 300 pA. During the elemental analysis of the surface the accelerating

Received: June 28, 2017
Revised: August 28, 2017
Published: August 30, 2017

DOI: 10.1021/acs.energyfuels.7b01856
Energy Fuels 2017, 31, 11253−11257

Table 1. Physical Properties of Ashalcha Heavy Oil at 20 °C

			elemental content (%)				SARA analysis (%)			
viscosity (mPa·s)	density (g·cc^{-1})	API gravity	C	H	N	S	saturated	aromatic	resins	asphaltenes
11 811	0.97	13.8	82.09	10.12	0.63	2.65	26.2 ± 0.5	44.1 ± 0.6	26.3 ± 0.5	4.5 ± 0.3

voltage of incident electrons was 5 kV, and working distance was 9 mm. Probing depth was about 1 μm.

2.2.3. X-ray Powder Diffraction. X-ray powder diffraction (XRPD) studies were made using a MiniFlex 600 diffractometer (Rigaku) equipped with a D/teX Ultra detector. Cu Kα1 radiation (40 kV, 15 mA) was used, and data were collected at 25 °C in the range of 2θ from 2° to 100° with a step of 0.02° and exposure time at each point of 0.24 s without sample rotation.

2.2.4. Specific Surface Area Measurements. Specific surface area (SSA) of the catalyst was measured by nitrogen adsorption at 77 K with an ASAP 2020 MP (Micromeritics) instrument. About 0.5 g of sample was degassed by heating at 200 °C under low pressure of 8 μmHg for 2 h. The SSA value was determined by applying the Brunauer–Emmett–Teller (BET) equation.

3. RESULTS AND DISCUSSION

It is widely known that phase content and morphological properties of the heterogeneous catalysts influence their performance. Therefore, primarily we studied characteristics of the synthesized catalyst in depth. It turns out that the applied synthetic procedure allows us to obtain highly crystalline manganese oxide(II) particles without any impurities of other manganese oxides as proved by XRPD analysis (Figure 1).

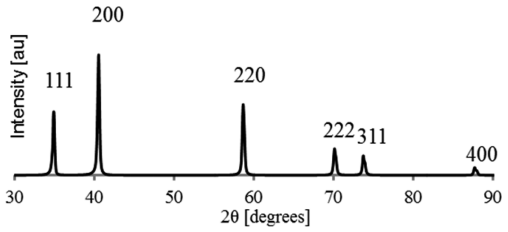

Figure 1. XRPD analysis of synthesized MnO submicroparticles.

To examine the size and morphology of obtained particles we applied scanning electron microscopy (SEM), which revealed (Figure 2) microcrystals possessing a form of octahedron (Figure 2 inset) with average size of 120 ± 34 nm (random edge length calculated from 100 measurements). Energy dispersive X-ray analysis (EDX) of microparticles' surface showed presence of carbon from oleic acid (Figure 3).

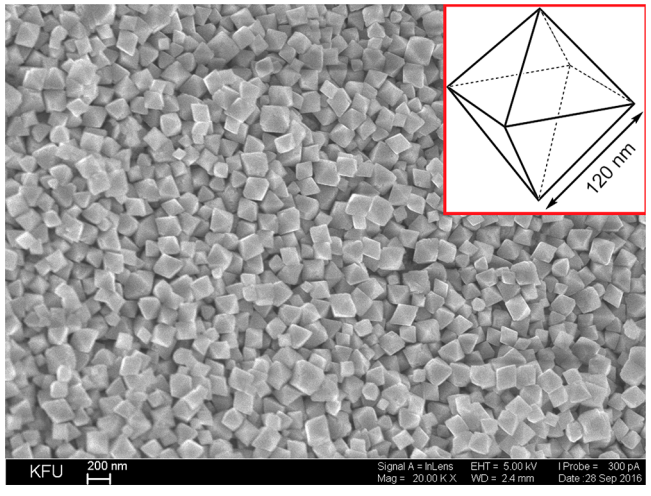

Figure 2. SEM image of synthesized MnO submicroparticles.

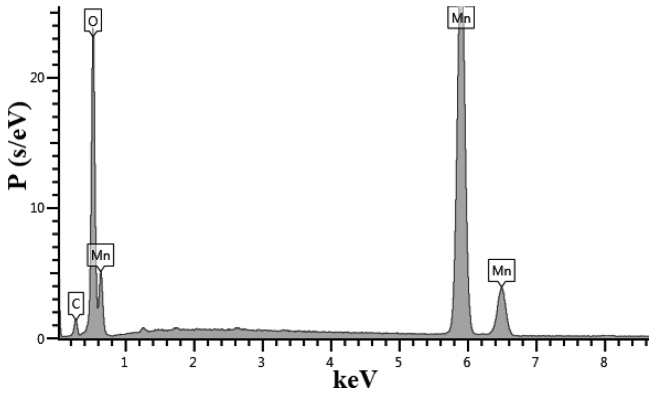

Figure 3. EDX spectrum of synthesized MnO submicroparticles.

We also used TG analysis to evaluate content of the oleic acid on the surface of the obtained submicroparticles. Total mass loss during heating procedure was 3.3%. As we can see (Figure 4), at the first step insignificant mass loss related to

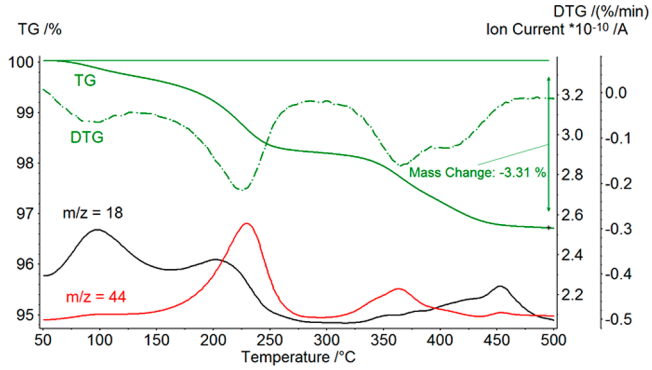

Figure 4. TG, DTG, and ion current curves for synthesized MnO submicroparticles (argon atmosphere, heating rate of 10 K·min^{-1}).

removal of physically adsorbed water (about 0.3%) takes place. At the second step, we observe simultaneous decarboxylation of oleic acid and removal of chemically adsorbed water. Total decomposition of organic matter occurs at the third step. As we can see, total decomposition of the organic part of the catalyst in argon atmosphere ends up at a temperature of about 450 °C, where we can consider the surface of our catalyst free of organic surfactant. In air atmosphere this process likely proceeds faster and ends up at a lower temperature.

Specific surface area is a very important characteristic determining activity of dispersed catalysts; therefore, we conducted nitrogen adsorption measurements to evaluate SSA of synthesized submicroparticles. Figure 5 shows nitrogen adsorption and desorption isotherms; the obtained SSA value was 12.85 ± 0.19 m^2·g^{-1}.

DOI: 10.1021/acs.energyfuels.7b01856
Energy Fuels 2017, 31, 11253–11257

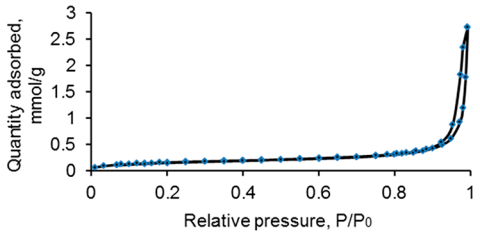

Figure 5. Nitrogen adsorption−desorption isotherms at 77 K.

The theoretical value of SSA calculated with assumption that submicroparticles have a form of right octahedron with an edge size of 120 nm (Figure 2) yields an SSA value of 11.28 $m^2 \cdot g$ (density of the MnO is assumed to be 5.43 $g \cdot cm^{-3}$). The closeness of the theoretical and measured SSA values evidences the nonporous nature of the catalyst, which is in good agreement with the results obtained by SEM. On the basis of the known catalyst's SSA value (12.85 $m^2 \cdot g^{-1}$), content of oleic acid (3%), and its molecular mass (282.5 $g \cdot mol^{-1}$), one can calculate the amount of surfactant molecules per 1 nm^2 of the catalyst surface, which is 5.1 $molecules \cdot nm^{-2}$. The cross-sectional area of oleic acid[12] is 0.46 nm^2, meaning that the average amount of oleic acid on a surface cannot exceed 2.2 $molecules \cdot nm^{-2}$ in the case of monolayer coverage. Thus, we guess that the surfactant covers the surface of the obtained MnO particles by 2−3 layers.

3.1. Combustion Study by DSC and Kinetic Analysis.

DSC curves related to noncatalytic and catalytic combustion of heavy crude oil performed at different heating rates are given in Figure 6. During combustion, two main oxidation regions, namely low-temperature oxidation (LTO) and high-temperature oxidation (HTO), are clearly seen on DSC curves. LTO yields partially oxygenated hydrocarbons (peroxides, alcohols, carbonyl compounds) without producing significant amount of carbon oxides.[13] HTO is usually described as coke oxidation producing carbon oxides and water.[14]

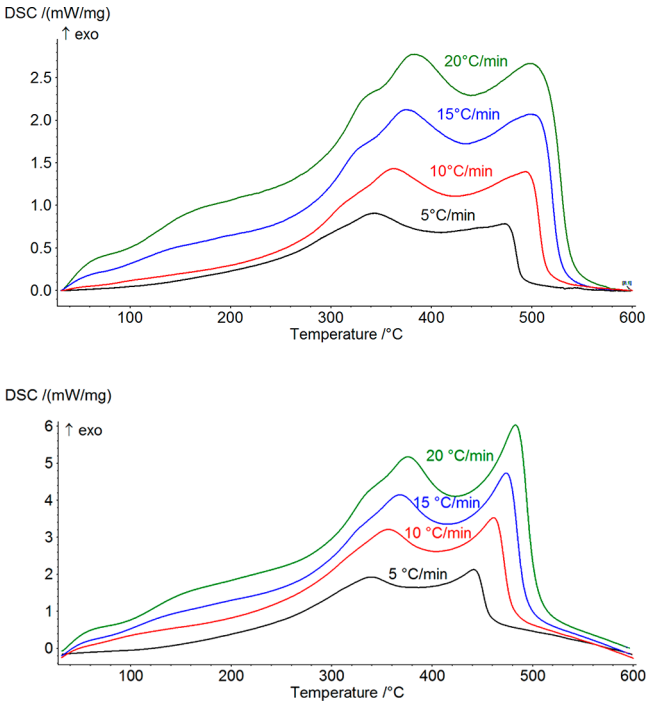

Figure 6. DSC curves for noncatalytic (top) and catalytic (bottom) heavy oil combustion.

DSC reaction intervals of both regions for noncatalytic and catalytic processes as well as peak temperatures are given in Table 2.

Table 2. DSC Reaction Intervals and Peak Temperatures

		noncatalytic		catalytic	
sample	β (°C × · min^{-1})	interval (°C)	T_p (°C)	interval (°C)	T_p (°C)
LTO	5	248−380	343	267−364	340
	10	276−409	364	257−383	358
	15	280−422	376	282−397	369
	20	291−426	386	297−406	377
HTO	5	433−489	473	422−457	441
	10	439−514	494	436−477	462
	15	444−528	502	446−493	474
	20	450−538	512	458−503	483

It can clearly be seen that peak temperatures of LTO regions are quite close to each other for corresponding heating rates for noncatalytic and catalytic processes, whereas peak temperatures of catalytic HTO are significantly lower. Figure 7 shows the differences between corresponding pairs of T_p values for low- and high-temperature oxidation.

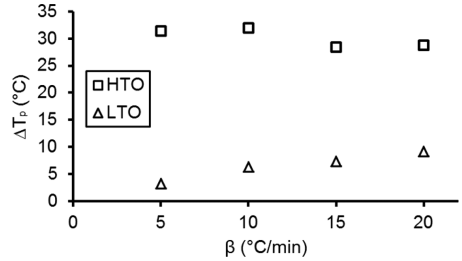

Figure 7. Differences between the peak temperatures (ΔT_p) for catalytic and noncatalytic heavy oil oxidation at different heating rates.

Oil oxidation can be described as a simple reaction rate model that assumes functional dependency on oil conversion degree, α, and oxygen partial pressure.[13] This widely accepted model is given by eq 1:

$$\frac{d\alpha}{dt} = k(T)P_{O_2}{}^{a}(1-\alpha)^{b} \quad (1)$$

The rate constant $k(T)$ is assumed to obey Arrhenius law (eq 2):

$$k(T) = Ae^{-E/RT} \quad (2)$$

The conversion degree α in DSC is calculated according eq 3:

$$\alpha = \frac{\int_{t_0}^{t}(dH/dt)dt}{\int_{t_0}^{t_f}(dH/dt)dt} \quad (3)$$

An early study conducted by Bousaid and Ramey shows a first-order dependency with respect to both oil concentration and oxygen partial pressure.[15] Because of the small amount of oil used for each DSC run in our study (about 1 mg) and high air flow rate of 75 mL/min combined with large furnace volume (approximately 250 mL), we assume that oxygen partial pressure remains constant (21.2 kPa) during the experiment.

DOI: 10.1021/acs.energyfuels.7b01856
Energy Fuels 2017, 31, 11253−11257

Considering all the above we express the final reaction model as described in eq 4.

$$\frac{d\alpha}{dt} = k_{eff}(1 - \alpha) \tag{4}$$

where

$$k_{eff} = kP_{O_2}$$

We used Kissinger's method[16] to study the kinetics of the heavy oil combustion. The method links variation of peak temperature from heating rate with kinetic parameters of the process; the logarithmic form of the equation is presented in eq 5.

$$\ln\frac{\beta}{T_p^2} = -\frac{E}{R} \times \frac{1}{T_p} + \ln\frac{A \times R}{E} \tag{5}$$

Kissinger's method was chosen over various of other integral and differential methods because of strong dependence of DSC data from the baseline choice. Because T_p values are almost independent of baseline choice, the Kissinger's method was the best alternative. Figure 8 shows Kissinger's plots for low- and high-temperature oxidation in the presence and absence of the catalyst. The kinetic parameters are grouped in Table 3.

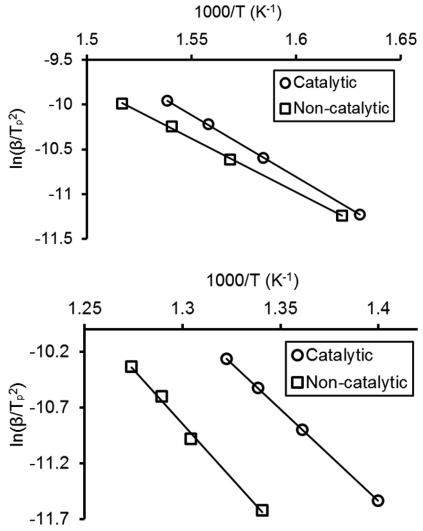

Figure 8. Kissinger's plots for catalytic and noncatalytic high temperature oxidation (top is for LTO, bottom is for HTO).

Table 3. Kinetic Parameters of Combustion Processes

	noncatalytic		catalytic	
	LTO	HTO	LTO	HTO
E_a (kJ/mol)	100.0 ± 1.8	161.7 ± 8.3	115.0 ± 0.7	137.1 ± 0.1
lg$A$	4.6	7.6	6.1	6.2

It should be noted calculated A and E_a parameters make opposite contributions into reaction rate constant $k(T)$ for both LTO and HTO processes. In the case of LTO, the catalytic process possesses higher E_a (which decreases $k(T)$) and higher preexponential factor A (which increases $k(T)$) compared with noncatalytic reaction. A similar situation occurred for HTO: the catalytic process possesses lower E_a (increasing $k(T)$) and lower A (decreasing $k(T)$) compared with noncatalytic reaction. To estimate the combined effect of these two parameters, we calculated $k(T)$ values for LTO and HTO over broad temperature ranges where these processes occurred (Table 2). Comparison of effective rate constants for noncatalytic and catalytic oxidation process is presented in Figure 9.

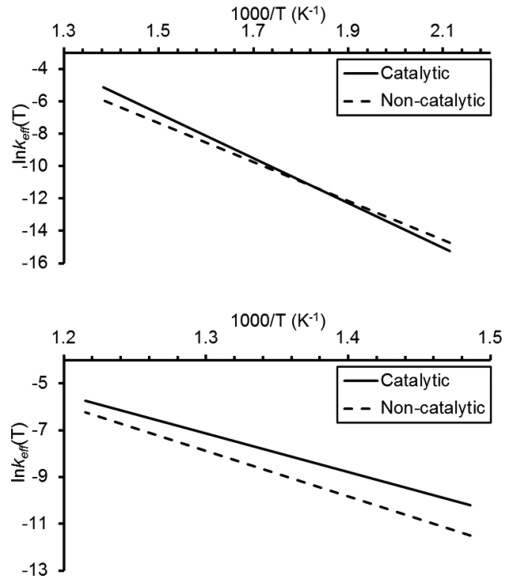

Figure 9. Variation of effective rate constants with temperature for catalytic and noncatalytic oxidation (top is for LTO, bottom is for HTO).

As we can see from Figure 9, noncatalytic and catalytic combustion show minimal differences for LTO, whereas in the case of HTO, the catalytic combustion rate is significantly higher. Thus, we can conclude that proposed Mn-based submicroparticles effectively catalyze the heavy crude oil oxidation process and might be applied for stabilization of the combustion front. Based on the results published in our previous study,[8] we propose MnO submicroparticles in the experiment's conditions transform into Mn_3O_4 which is supposed to be the real catalyst.

4. CONCLUSIONS

We synthesized manganese oxide(II) submicroparticles stabilized with oleic acid and studied their composition, size, and morphological properties in depth. We applied nonisothermal kinetic analysis coupled with an isoconversional approach to study the influence of catalyst on combustion process and showed that synthesized Mn-based submicroparticles accelerate predominantly the high-temperature oxidation process. Further improvement of catalytic performance may be reached by adjustment of size and morphology of the particles to increase surface area available for reaction, which is a theme of our future study.

AUTHOR INFORMATION

Corresponding Author

*E-mail: and_galuhin@mail.ru.

ORCID

Andrey V. Galukhin: 0000-0003-3077-3816

Funding

The work was supported by Grant No.14.Y26.31.0019 from Ministry of Education and Science of Russian Federation.

DOI: 10.1021/acs.energyfuels.7b01856
Energy Fuels 2017, 31, 11253−11257

Notes

The authors declare no competing financial interest.

REFERENCES

(1) Rein, G. *Fire Phenomena and the Earth System: An Interdisciplinary Guide to Fire Science*; John Wiley & Sons: Oxford, 2013; pp 15−34.
(2) Baud, G.; Salvador, S.; Debenest, G.; Thovert, J.-F. *Energy Fuels* **2015**, *29*, 6780−6792.
(3) Abuhesa, M. B.; Hughes, R. *Energy Fuels* **2009**, *23*, 186−192.
(4) Piumetti, M.; Fino, D.; Russo, N. *Appl. Catal., B* **2015**, *163*, 277−287.
(5) Santos, V.; Pereira, M.; Orfao, J.; Figueiredo, J. *Appl. Catal., B* **2010**, *99*, 353−363.
(6) Kuwahara, Y.; Yoshimura, Y.; Yamashita, H. *Catal. Sci. Technol.* **2016**, *6*, 442−448.
(7) Huang, G.; Luo, J.; Deng, C. C.; Guo, Y. A.; Zhao, S. K.; Zhou, H.; Wei, S. *Appl. Catal., A* **2008**, *338*, 83−86.
(8) Galukhin, A. V.; Khelkhal, M. A.; Gerasimov, A. V.; Biktagirov, T.; Gafurov, M. R.; Rodionov, A.; Orlinskii, S. B. *Energy Fuels* **2016**, *30* (9), 7731−7737.
(9) Galukhin, A.; Erokhin, A.; Osin, Y.; Nurgaliev, D. *Energy Fuels* **2015**, *29* (8), 4768−4773.
(10) Biktagirov, T.; Gafurov, M.; Mamin, G.; Gracheva, I.; Galukhin, A.; Orlinskii, S. *Energy Fuels* **2017**, *31* (2), 1243−1249.
(11) Schladt, T. D.; Graf, T.; Tremel, W. *Chem. Mater.* **2009**, *21*, 3183−3190.
(12) Ma, J. K. H.; Hadzija, B. *Basic Physical Pharmacy*; Jones & Bartlett: Burlington, MA, 2012; pp 284−285.
(13) Sarathi, P. *In-situ Combustion Handbook: Principles and Practices*; National Technology Information Service: Bartlesville, OK, 1999; pp 42−43.
(14) Khansari, Z.; Gates, I. D.; Mahinpey, N. *Fuel* **2014**, *115*, 534−538.
(15) Bousaid, I.; Ramey, H. *SPEJ, Soc. Pet. Eng. J.* **1968**, *8*, 137−148.
(16) Kissinger, H. *J. Res. Natl. Bur. Stan.* **1956**, *57*, 217−221.

DOI: 10.1021/acs.energyfuels.7b01856
Energy Fuels 2017, 31, 11253−11257